09

Compound X-ray amorphous radiation-cooled filter based on free-standing thin films for synchrotron radiation facilities

© Yu.V. Khomyakov,[1] Ya.V. Rakshun,[1,2] M.V. Gorbachev,[3] O.M. Kutkin,[3] V.A. Chernov[1]

[1] Budker Institute of Nuclear Physics, Siberian Branch, Russian Academy of Sciences,
630090 Novosibirsk, Russia
[2] Siberian State University of Telecommunications and Information Science,
630102 Novosibirsk, Russia
[3] Novosibirsk State Technical University,
630073 Novosibirsk, Russia
e-mail: yu.v.khomyakov@yandex.ru

Received May 17, 2024
Revised May 17, 2024
Accepted May 17, 2024

A radiation-cooled X-ray amorphous filter based on thin films is proposed for use at 4th generation synchrotron radiation facilities' beamlines. This filter can be exploited under conditions of high thermal loads and high coherent photon flux fraction. In order to ensure X-ray amorphousness, it is proposed to use glassy carbon, metallic glasses, and multilayers with nano-sized periods as filter materials. Filtering is assumed to be carried out in stages: first, radiation in the low-energy range (up to ~ 5 keV), and then, if necessary, in the medium-energy range (up to ~ 15 keV) being suppressed. It is proposed to use a set of glassy carbon films as an absorber for primary filtering and a set of films containing elements with higher atomic numbers for additional filtering. The selection of filter film materials allows for consistent suppression of undulator harmonics when operating in the high-energy range (above 15 keV). Modeling of thermal loads and stationary temperature distribution has been carried out for glassy carbon films. The thickness of these radiation-cooled films is chosen in such a way that their maximum temperature in thermal equilibrium does not exceed the graphitization temperature.

Keywords: X-ray filter, X-ray amorphousness, radiative cooling, synchrotron radiation, undulator radiation.

DOI: 10.61011/TP.2024.07.58817.178-24

Introduction

Ultra low emittance close to the diffraction limit is the key feature of new fourth-generation synchrotron radiation (SR) facilities. Electron bunches circulating in the storage rings of such facilities generate intensive X-ray beams with small angular divergence, relatively high photon flux coherent fraction and large spatial coherence lengths. The specified radiation properties enable the new „coherent" methods of substance investigation to be used. Nevertheless, to implement the potential of the modern SR facilities, specialized X-ray optics, in particular, filters shall be developed.

Hard X-ray experiments at SR facilities with a relatively low electron energy (3 GeV and lower) are performed using high harmonics of undulators (Figure 1). And it turns out to be necessary to suppress the first high-intensity long-wavelength undulator harmonics to avoid overheating of the X-ray optical elements of beamlines. Therefore, cooled filters are placed upstream of beamline optics.

In the storage rings of the fourth-generation SR facilities, total power emitted by electrons going through the undulator's magnetic field achieves tens of kilowatts. After preliminary collimation, the undulator radiation (UR) power is equal to hundreds or even thousands of watts. Whereas the lateral size of undulator beams in question is about 1 mm. Thus, the primary filtering elements on modern undulator beamlines are exposed to extremely high local heat loads, thus, giving rise to a nontrivial heat removal problem.

One of the solutions is the use of single-crystal diamond as a primary filtering element [1]. Due to its record-breaking high thermal conductivity, the diamond single-crystal withstands extremely high heat fluxes, however, UR flow through the single-crystal results in occurrence of unwanted Bragg reflections at some wavelengths which hinders or even prevents the use of radiation at such wavelengths. In other words, the spectrum of UR that has passed through the single-crystal becomes riddled with so-called „glitches" [2], i.e. dips corresponding to crystal diffraction.

Another widely used primary filter material is graphite because it also withstands extremely high temperatures [3]. Nevertheless, the use of such filter results in spurious interference when partially coherent UR passes through a polycrystalline substance. Visibility of the occurring unwanted fringe pattern depends heavily on the crystal grain sizes. The material consisting of crystallites of several tens of nanometers in size may be considered as X-ray amorphous [4]. Then, when using a nanocrystalline carbon filter [5] in high thermal load conditions, it is required to avoid recrystallization. Moreover, transition to nanocrystalline materials means considerable reduction

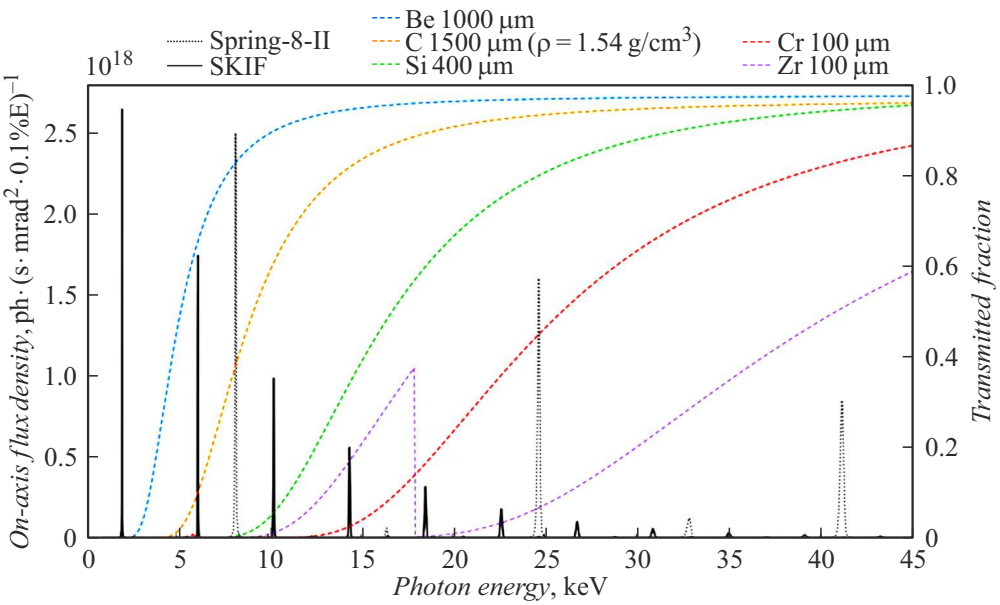

Figure 1. Comparison of radiation spectra generated by the same undulator (Table 1) installed on a straight section of Spring-8-II (electron energy 6 GeV, [7]) and SKIF (3 GeV, [8]) storage rings. transmittances of some filters are listed — the selected filter materials and thicknesses provide successive suppression of UR harmonics in a high-energy range.

Table 1. Storage ring and superconducting undulator parameters used for calculations

Parameter	Value
Storage ring	
Electron energy, GeV	3
Beam current in the main mode, mA	400
Horizontal beta-function in the center of the straight section, m	15.6
Vertical beta-function in the center of the straight section, m	2.4
Horizontal emittance in the main mode (with full current), pm·rad	68.18
Vertical emittance in the main mode (with full current), pm·rad	6.818
Horizontal electron bunch size in the center of the straight section $\sigma_x = \mathrm{FWHM}_x/2.355$, μm	32.6
Vertical electron bunch size in the center of the straight section $\sigma_y = \mathrm{FWHM}_y/2.355$, μm	4.02
Superconducting undulator	
Period, mm	15.6
Peak magnetic field, T	1.25
Number of periods	128

of thermal conductivity which aggravates the heat removal problem. Thus, for example, thermal conductivity of natural diamond at room temperature is higher than that of nanocrystalline diamond with a grain size of 10 nm by 2 orders of magnitude, and of 6 nm — by 3 orders of magnitude [6].

At operating energies higher than 30 keV, multilayer mirror monochromators used on the SR facility beamlines transmit radiation in low- and medium-energy portions of spectrum due to the total external reflection (TER) phenomenon. For suppression, absorbers made of material containing elements with higher atomic numbers are inserted (Figure 1). Even considering the collimation and primary filtration, thermal loads on these additional filters turn out to be extremely high resulting in the same problems as that described for the primary filter.

A concept of X-ray amorphous radiation-cooled thin-film filter is offered herein. Such X-ray filter, on the one hand, is

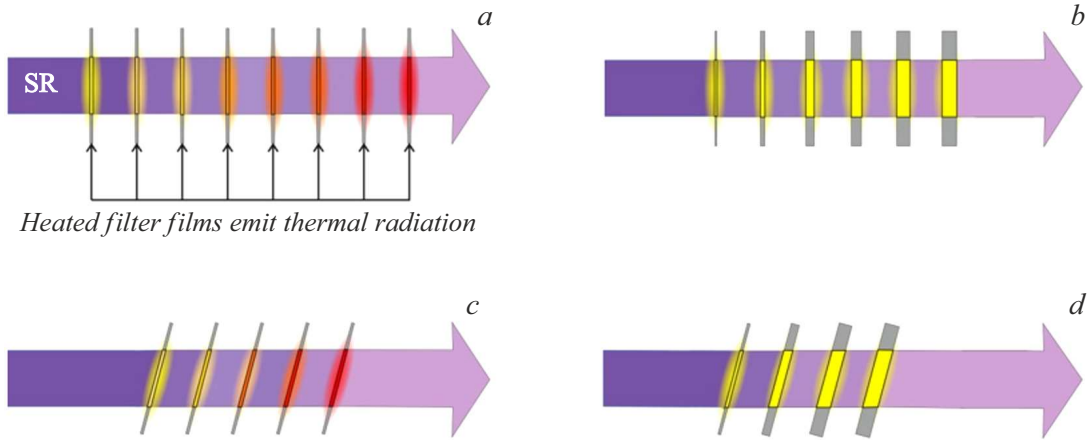

Figure 2. Radiation-cooled X-ray filter based on thin films in various versions: *a* — with normal incidence and constant film thickness; *b* — with normal incidence and growing film thickness; *c* — with incidence at angle θ to surface and constant film thickness; *d* — with incidence at angle θ to surface and growing film thickness.

able to withstand high thermal loads and, on the other hand, does not induce spurious diffraction and interference and, therefore, is important for modern SR facility beamlines.

1. Operating principle of the radiation-cooled filter

Operating principle of the given X-ray amorphous filter is shown in Figure 2. The system consists of a set of filtering elements — spaced-apart free-standing thin films that together provide the necessary thickness of the filtering substance. It is proposed to make films from glassy carbon, metallic glasses, multilayers or other X-ray amorphous materials. In case of a multilayer, low thickness of layers is chosen (units of nanometers in the order of magnitude), whereas interlayer boundaries prevent crystallite growth. When the SR beam passes through the filter, the absorbing films are heated until thermal equilibrium is achieved, i.e. to the temperature at which the absorbed X-rays power becomes equal to the emitted thermal radiation power. To ensure efficient heat removal, the films are quite spaced apart. Thickness of an individual film is selected such that to minimize the total number of filtering elements, but to avoid overheating.

The proposed radiation-cooled thin-film filter may be available in various versions. In the simplest case, films with the same thickness are placed at right angle to incident UR (Figure 2, *a*). In order to minimize the number of filtering element or for smooth variation of the filter transmittance, the films may be inclined as shown in Figure 2, *c*. In this case, the power absorbed by each film will increase, but surface and volume densities of absorbed power will change just a little, which will be demonstrated below. Modification of both versions described above is possible to make the device more compact: film thicknesses may be increased

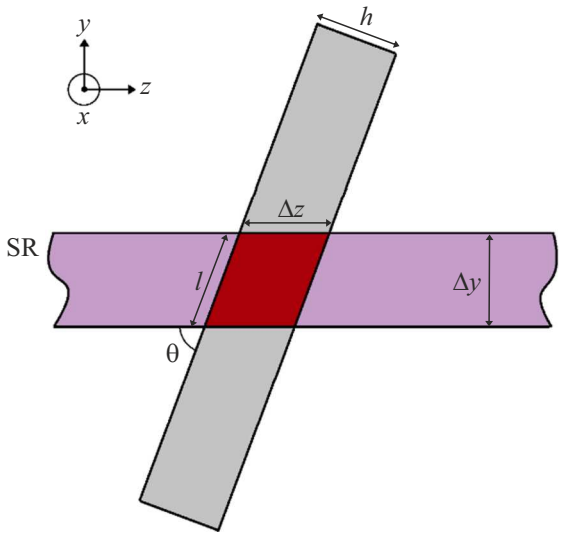

Figure 3. Illustration to the inclined filter problem.

with UR attenuation in such a way as to maintain the same steady-state peak temperature of the films (Figure 2, *b, d*).

It is important that the EUV lithography has successful experience of long-term application of radiation-cooled thin-film screens — pellicles. Power absorbed by one such screen may achieve tens of watts at a density of absorbed power of about 1 W/cm^2, and the pellicle is heated up to temperatures of about one thousand degrees [9,10].

Let us consider in more detail the problem of the effect of film inclination with respect to the SR beam on the film absorptance. Assume that a parallel monochromatic X-ray beam with the wavelength λ and lateral sizes $\Delta x \times \Delta y$ passes through a film with the thickness h with refraction index $n = 1-\delta-i\beta$ at the angle θ to the surface (Figure 3). Then, the substance layer thickness through which radiation passes is equal to $\Delta z = \frac{h}{\sin\theta}$, and the size of the illuminated

area on the film surface is $\Delta x \times l$, where $l = \frac{y}{\sin\theta}$. Photon flux Φ, i.e. the number of photons flowing through the area $\Delta x \times \Delta y$ per unit time, decreases exponentially with the substance depth z under the Bouguer–Lambert–Beer law:

$$\Phi(z) = \Phi_0 \exp(-\mu z), \tag{1}$$

where Φ_0 — is the photon flux before absorption, μ — is the linear absorption coefficient of this substance for λ. Full number of absorbed photons per unit time:

$$\Phi_{abs} = \Phi_0 - \Phi(\Delta z) = \Phi_0 \left[1 - \exp\left(-\frac{\mu h}{\sin\theta}\right)\right]. \tag{2}$$

Film substance volume in which absorption takes place:

$$V = \Delta x \Delta y \Delta z = \frac{\Delta x \Delta y h}{\sin\theta}. \tag{3}$$

Then from (2) and (3), the averaged volume density q_v and surface density q_s of absorbed power are expressed as

$$\overline{q}_v = \frac{\Phi_{abs} E_{\text{ph}}}{V} = \frac{1}{\Delta x \Delta y h} \frac{2\pi\hbar c}{\lambda} \Phi_0 \sin\theta \left[1 - \exp\left(-\frac{\mu h}{\sin\theta}\right)\right], \tag{4}$$

$$\overline{q}_s = \overline{q}_v h,$$

where $E_{\text{ph}} = \frac{2\pi\hbar c}{\lambda}$ is the photon energy.

Note that for the wavelength of X-rays absorbed by the filter $\lambda = 0.5\,\text{nm}$ and for the typical (as shown in Section 3) film thickness of $h = 250\,\text{nm}$, we have

$$\mu h = 4\pi\beta \frac{h}{\lambda} \sim 4\pi \cdot 10^{-6} \frac{250\,\text{nm}}{0.5\,\text{nm}} \sim 10^{-2} \ll 1.$$

Now assume $\theta \sim 1\,\text{rad}$ (i.e. not the grazing incidence case) and, by expanding (4) in series in $\frac{\mu h}{\sin\theta} \sim \mu h \ll 1$, we obtain

$$\overline{q}_v \propto \frac{\sin\theta}{h} \left[1 - 1 + \frac{\mu h}{\sin\theta} - \frac{1}{2}\left(\frac{\mu h}{\sin\theta}\right)^2\right] = \mu \left[1 - \frac{1}{2}\frac{\mu h}{\sin\theta}\right]. \tag{5}$$

Expression (5) shows that the averaged density of absorbed power decreases slowly with θ. Considering this density as constant, now we obtain the absorbed and reradiated powers

$$P_{abs} = \overline{q}_v V \propto \frac{1}{\sin\theta}, \tag{6}$$

$$P_{rad} = 2\varepsilon\sigma T^4 l \Delta x \propto \frac{1}{\sin\theta},$$

where ε — is the emissivity factor, σ — is the Stefan–Boltzmann constant, T — is the temperature of radiated film surfaces.

Thus, for one film to a first approximation (non-grazing incidence), $\overline{q}_v, \overline{q}_s$ and T do not depend on the angle of incidence in the thermal equilibrium state. However, when θ decreases, the effective filter thickness increases by a factor of $1/\sin\theta$ which corresponds to the decrease in the required number of films. Unlike this, films with higher thickness $h^* = h/\sin\theta$ placed normally to the UR beam result in thermal equilibrium temperature growth as shown in (6): power absorbed by each individual film increases and the heating spot area, i.e. the intensively radiating film surface area, remains minimum.

Note that the proposed concept of a composite filter allows some film defects. Assume that the i-th film of the filter has a through hole with a small diameter, then the ray going through this hole will lead in phase the rays passing through the film.

$$\Delta\varphi_i = 2\pi \frac{\delta h}{\lambda \sin\theta}. \tag{7}$$

Take glassy carbon with a density of $1.54\,\text{g/cm}^3$ as an example of film material. With normal incidence of X-rays at an operating wavelength of $\lambda = 0.1\,\text{nm}$ on the $250\,\text{nm}$ glassy carbon film, we have

$$\Delta\varphi_i = 2\pi \frac{2.1 \cdot 10^{-6}\, 250\,\text{nm}}{0.1\,\text{nm}} \approx 2\pi \cdot 0.005 < \pi/2.$$

In other words, the wavefront aberration remains within the Rayleigh tolerance $\lambda/4$ with a margin of safety. It can be reasonably suggested that random positions of defect will be evenly distributed over the area of each filter film and the probability that several defects on different films will occur on the same ray path is low. Then, when passing through all films, the wavefront aberration will also remain lower than $\lambda/4$.

Suitability of thin multilayer films at grazing angles to UR shall be addressed separately. Due to the Bragg diffraction on the multilayer, a device with such geometry could selectively reflect radiation in the specified narrow wavelength range slightly decreasing the intensity in the remaining spectrum. Film arrangement at different angles within the filter unit or the employment of various multilayers would allow for X-rays „equalization“ to be organized, i.e. to give any pre-defined shape of the dependence of the filter transmittance on energy. Nevertheless, achievement of the flatness of such thin film within the boundaries of the illuminated area that is necessary to satisfy the Bragg condition presents an extremely nontrivial problem, especially considering the highest thermal loads. Another potential area for the development of thin-film filters could be the implementation of the TER phenomenon to extract the low-energy portion of radiation from the beam, for which, however, the films must have been placed at even lower grazing angles to X-rays.

The proposed thin-film filter can perform a set of additional functions on SR facility beamlines. The device can be used for monitoring of the X-ray beam intensity, shape, sizes, position and direction by thermal radiation. For this, a couple of thermal imaging cameras shall be directed through sight glasses to the first and last filtering films. Relatively sharp boundaries of the beam footprint will be distinguished on the recorded temperature maps (shown in Section 3).

A single film may serve as a window in ultrahigh-vacuum channels. The whole film package, when using

the corresponding materials may play a role of gas absorber. Moreover, the proposed filter will reduce molecular conductivity of the vacuum channel.

2. Materials

A wide set of technologically available amorphous materials and multilayers [11] will provide efficient selection of filters for various radiation ranges. It is expected that UR filtration will be performed in several stages using a filter combination. The primary filter may be installed in frontends of SR facility beamlines and the additional filters containing heavier chemical elements will be inserted into the beam, if required. Certainly, to ensure long-term thermal stability, heat-resistant absorbing film materials shall be chosen for all filters.

The primary filter is designed to absorb mainly low-energy portion of spectrum, therefore, the primary filter films shall be made from a material with a low atomic number. Glassy carbon and multilayers based on beryllium, boron, carbon, nitrogen and oxygen, for example, B_4C/BeO_x, C/BN, etc., are among the candidates for such material. For example, thermally stable multilayer $TiAlN/Si_3N_4$ [12], Sc/CrN_x [13] or SiC/Be films may be used for additional filtration. For a harder range, multilayers with heavier chemical elements may be used such as WC_x/B_4C [14] and refractory metallic glasses based on Mo, Zr, W, Re [15], etc.

Filtering films may be placed in vacuum or in nitrogen and noble gas atmosphere, including He, Ne, Ar, Kr, Xe. In case of gas atmosphere, cooling due to partial heat transfer to the gas flowing around the films will be added to the radiation cooling mechanism. Moreover, smooth variation of the filter transmittance will be available by means of gas pressure adjustment in the chamber.

3. Simulation

For performance check of the thin-film radiation-cooled X-ray filter, UR spectra, thermal loads and film temperature distribution were calculated in thermal equilibrium state. The calculations use the parameters of the storage ring [8] and superconducting undulator of 1−1 Microfocus [16] beamline of SKIF fourth-generation SR facility (Table 1). It is assumed that the generated UR beam is collimated before passing through the filter unit: in the beamline frontend, an angular aperture $(75\,\mu\text{rad})^2$ is pre-defined by masks.

Figure 4 shows the spectrum of the photon flux emitted into a solid angle of $(75\,\mu\text{rad})^2$ upstream of filters, downstream of the glassy carbon filter with a total thickness of $1750\,\mu$m, downstream of the double-mirror multilayer monochromator (DMM) set to transmission of 30.9 keV, and downstream of DMM with inserted additional SiC filter with a total thickness of $300\,\mu$m. The required thickness of the primary filter is provided by combining ~ 1000 glassy carbon thin films package that accept the highest thermal load and glassy carbon plates placed downstream of it. At high energies, the DMM mirrors [17] are placed at grazing angles $\sim 0.5^\circ$ to the beam due to which DMM transmits low-energy harmonics of the undulator as a result of the TER phenomenon. Additional $300\,\mu$m SiC filter ensures suppression of these spurious harmonics by reducing considerably the thermal load on the downstream X-ray optics of the beamline. The required thickness of SiC is provided by the SiC/Be multilayer film package.

To estimate heat fluxes on the evacuated primary filter, the absorbing glassy carbon films were hereinafter assumed to be homogeneous with a density of $\rho = 1.54\,\text{g/cm}^3$, which corresponds to the pyrolysis temperature of 1373 K (SIGRADUR® K, [18]). Glassy carbon made at higher temperatures (about 2473 K) has graphite impregnations and cannot be considered as amorphous, therefore it was not included in the calculation. The distance from the center of undulator to the primary filter was set to 20 m.

The first part of Table 2 describes the UR absorption by the first glassy carbon film of the primary filter in case of normal incidence, and different film thicknesses are addressed. For further calculation, a thickness of 230 nm was chosen, UR absorption by the first ten such films is described in the second part of Table 2. Film thickness was selected such that the thermal equilibrium was achieved at a temperature lower than the pyrolysis temperature of the chosen glassy carbon grade (1373 K): graphitization starts when this temperature is exceeded.

Figure 5 shows the section of volume density of absorbed power q_v at different film depths with normal UR incidence (Figure 5, *a*), and maps of the depth-averaged $h = 230$ nm surface density of absorbed power $\overline{q}_s$ with normal incidence (Figure 5, *b*) and incidence at 10° to the film surface (Figure 5, *c*). When the film is inclined, the integral power P_{abs} is increased from 0.5 to 2.9 W, i.e. by a factor of 5.8 (which corresponds to $1/\sin(10^\circ) \approx 5.8$), while the mean surface and volume densities $\overline{q}_s$ and $\overline{q}_v$ vary just a little. Heat flux distribution was calculated using SPECTRA software [19]. Further calculations addressed only the case of normal X-ray incidence.

In order to estimate the steady-state temperature distribution in the composite filter, a radiative heat exchange model problem was addressed as shown in Figure 6, *a*. To consider the effect of partial absorption of the emitted thermal radiation by adjacent films to a first approximation, the problem used the most thermally loaded first three filtering films of $h = 230$ nm in thickness, spaced apart at $\Delta = 5$ mm. In accordance with the second part of Table 2, homogeneous volume heat sources q_{v1}, q_{v2} and q_{v3} were set inside the films, because the density of absorbed power at the film depth varies weakly (Figure 5, *a*).

The thermal conductivity of the chosen glassy carbon grade weakly depends on temperature [18], it was set to a constant value $k = 6.5\,\text{W/(m}\cdot\text{K)}$ for the numerical

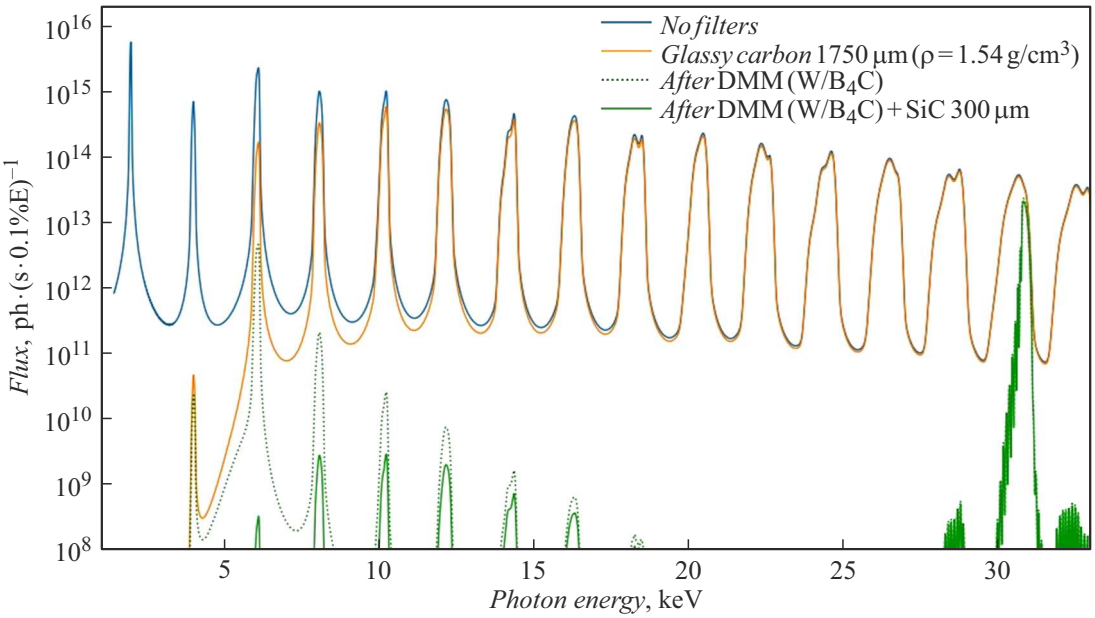

Figure 4. Attenuation of spurious „soft“ undulator harmonics. The calculation was performed using SPECTRA [19].

Table 2. Absorption in glassy carbon films at normal UR incidence. Illuminated area $(1.5\,\text{mm})^2$

Single films of different thickness				
Film thickness h, nm	Transmitted power, W	Absorbed power, W	Mean density of absorbed power $\overline{q}_v$, W/mm^3	Mean density of absorbed power $\overline{q}_s$, W/mm^2
230	298.85	0.49	941.55	0.22
460	298.36	0.97	937.68	0.43
920	297.41	1.93	929.96	0.86
1840	295.55	3.79	914.51	1.68
2300	294.64	4.69	906.78	2.09
Set of films with the same thickness $h = 230$ nm				
Film No.	Transmitted power, W	Absorbed power, W	Mean density of absorbed power $\overline{q}_v$, W/mm^3	Mean density of absorbed power $\overline{q}_s$, W/mm^2
1	298.85	0.487	941.55	0.22
2	298.36	0.483	933.82	0.21
3	297.88	0.479	926.09	0.21
4	297.41	0.475	918.37	0.21
5	296.94	0.471	910.64	0.21
6	296.47	0.467	902.92	0.21
7	296.01	0.463	895.19	0.21
8	295.55	0.459	887.47	0.20
9	295.09	0.455	879.74	0.20
10	294.64	0.451	872.01	0.20

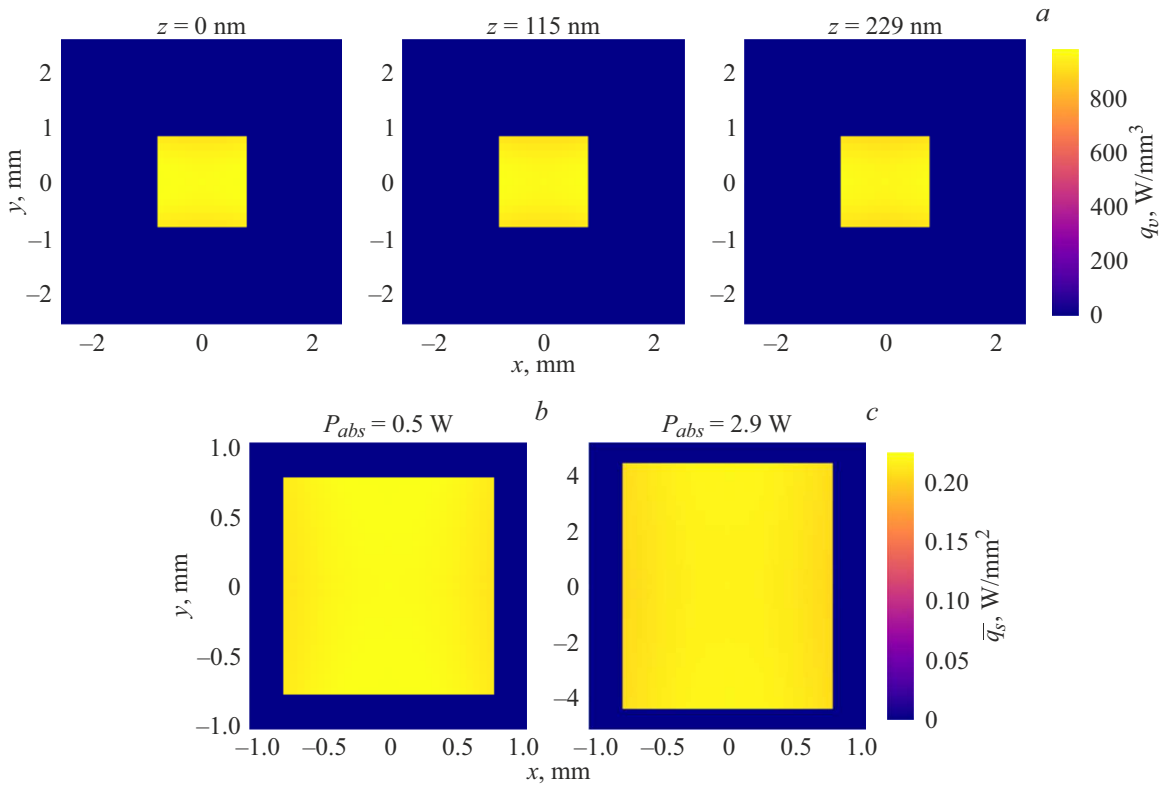

Figure 5. Power density maps of UR absorbed by the first $h = 230$ nm glassy carbon film: *a* — volume density q_v sections at different film depths with normal UR incidence; *b* — depth-averaged surface density $\overline{q}_s$ with normal UR incidence; *c* — depth-averaged surface density $\overline{q}_s$ with UR incidence at 10° to the surface.

Table 3. Steady-state temperature distribution calculation

Film No.	q_v, W/mm^3	Heat flux symbol	Radiated power, W	Total radiated power, W	Peak temperature, K
1	941.55	$q_{b\_1.1}$	0.22848	0.487	1182
		$q_{a\_1.1}$	0.04959		845
		$q_{b\_1.2}$	0.22091		1182
		$q_{a\_1.2}$	−0.01173		845
		q_{c_1}	0.00001		422
2	933.82	$q_{b\_2.1}$	0.22321	0.483	1184
		$q_{a\_2.1}$	0.01783		856
		$q_{b\_2.2}$	0.22323		1184
		$q_{a\_2.2}$	0.01897		856
		q_{c_2}	0.00001		473
3	926.09	$q_{b\_3.1}$	0.21724	0.479	1177
		$q_{a\_3.1}$	−0.01200		843
		$q_{b\_3.2}$	0.22459		1177
		$q_{a\_3.2}$	0.04942		843
		q_{c_3}	0.00001		420

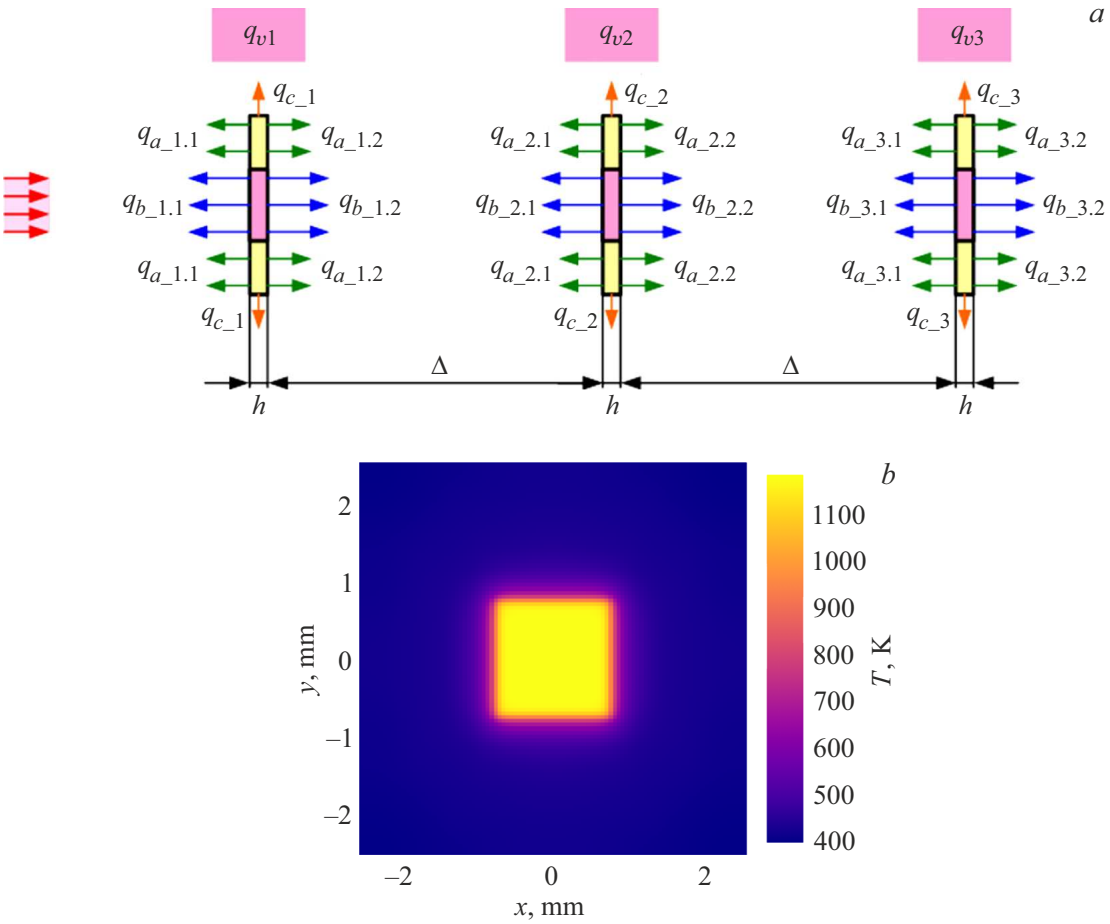

Figure 6. Radiative heat exchange in the composite filter consisting of 230 nm glassy carbon films: *a* — illustration to the model problem; *b* — calculated temperature distribution on the first film surface of the filter.

simulation. The surface emissivity factor of all films addressed herein was set to a constant value $\varepsilon = 0.65$ [20]. The steady-state temperature distribution was calculated in Fluent module of ANSYS 2020R2 software [21]. Calculated thermal radiation powers and maximum surface temperatures are listed in Table 3, the temperature map of the first film is shown in Figure 6, *b*.

Peak temperatures of the radiated films reach ~ 1200 K, which is below the initial active graphitization temperature of glassy carbon. This means that radiation cooling is quite efficient and the films retain their X-ray amorphousness. Thus, it is possible to use radiation-cooled glassy carbon films for the primary filtration of powerful UR.

For comparison, steady-state temperature distribution was also calculated for the case of one water-cooled „integral“ glassy carbon filter of 1750 μm in thickness as shown in Figure 7, *a*. Heat transfer coefficient 3000 W/(m$^2 \cdot$ K) at a water temperature of 295.15 K and a temperature-independent thermal conductivity of glassy carbon 6.5 W/(m $\cdot$ K) were set for the simulation. Thermal radiation emitted by the central section of the filter was considered, and constant emissivity factor was set to $\varepsilon = 0.65$. The volume heat source q_v was set considering the varying density of the absorbed UR power with the filter depth (Figure. 7, *b*).

Temperature distribution obtained in such simulation is shown in Figure 7, *c*. The maximum temperature of 6000 K exceeds even the graphite boiling temperature (4473 K). Actually heating will first result in local graphitization, and in this case thermal conductivity increases considerably and the thermal equilibrium temperature decreases. Even if the final temperature turns out to be lower than the graphite melting point (3925 K) and the filter remains hard, then it is no X-ray amorphous any longer.

Figure 7, *b* shows that the maximum thermal load is applied to the first $\sim 230\,\mu$m of the primary glassy carbon filter depth (72 W is absorbed in the first 230 μm, 144 W is integrally absorbed in 1750 μm). High volume densities of absorbed UR power in this near-surface layer correspond to absorption of the first intensive undulator harmonic. Therefore, it is feasible to use a combination of radiation-cooled filtering films and conventionally-cooled „thick“ filter: about 1000 films of 230 nm in thickness will accept the main thermal load, and the next glassy carbon plate will ensure the required thickness of the filtering substance.

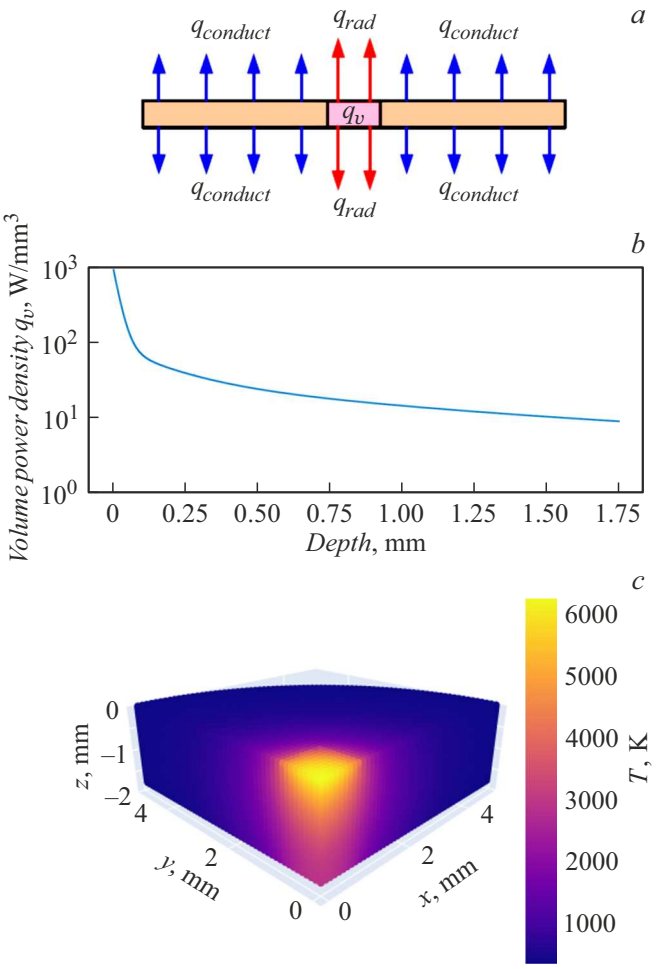

Figure 7. Water-cooled 1750 μm glassy carbon filter: *a* — illustration to the model problem; *b* — dependence of the volume density of absorbed UR power on the filter depth; *c* — calculated temperature distribution (one filter quadrant is shown).

Conclusion

An idea of a radiation-cooled X-ray amorphous thin-film filter for the fourth-generation SR facilities is described. Glassy carbon, refractory metallic glasses and potentially heat-resistant multilayers are proposed as filtering film materials. Simulation of thermal loads and steady-state temperature distribution for the primary glassy carbon filter has been performed. Film thickness was chosen to ensure the maximum film temperature in thermal equilibrium during radiation cooling not exceeding the graphitization temperature. The simulation indicates that radiation-cooled glassy carbon films are suitable for primary filtering of powerful UR at the fourth-generation SR facility beamlines. For successive suppression of UR harmonics in the high-energy X-ray range, additional filters with higher atomic numbers were proposed. Further it is planned to select the most promising materials and test their thermal stability experimentally.

It is worth noting that the addressed concept of radiation-cooled X-ray amorphous filter may be also used on wide wiggler beams having higher integral powers, but much lower flux densities.

Funding

The study was performed under State assignment No. FWGM-2022-0006.

Conflict of interest

The authors declare that they have no conflict of interest.

References

[1] S.V. Volkov, A.G. Elesin, K.V. Zolotarev, A.A. Krasnov, K.S. Lomakin, S.V. Mayoriv, S.N. Makarov, A.D. Nikolenko, V.N. Seroshtan, D.V. Skokov, A.V. Shevlyakov. V sb.: *Tekhnologicheskaya infrastruktura sibirskogo kol'tsevogo istichnika fotonov „SKIF“*, pod. red. K.I. Shifer (Institut kataliza SO RAN, Novosibirsk, 2022), s. 53–71. (in Russian)

[2] Q. Zhang, M. Polikarpov, N. Klimova, H.B. Larsen, R. Mathiesen, H. Emerich, G. Thorkildsen, I. Snigireva, A. Snigirev. J. Synchrotron Rad., **26** (1), 109 (2019). DOI: 10.1107/S1600577518014856

[3] A.M. Khounsary, P.J. Viccaro, T.M. Kuzay. SPIE, **1345**, 42 (1991). DOI: 10.1117/12.23301

[4] M. Yabashi, K. Tono, H. Mimura, S. Matsuyama, K. Yamauchi, T. Tanaka, H. Tanaka, K. Tamasaku, H. Ohashi, S. Goto, T. Ishikawa. J. Synchrotron Rad., **21**, 976 (2014). DOI: 10.1107/S1600577514016415

[5] H. Schulte-Schrepping, U. Hahn. AIP Conf. Proc., **879**, 1042 (2007). DOI: 10.1063/1.2436241

[6] M. Mohr, L. Daccache, S. Horvat, K. Brühne, T. Jacob, H. Fecht. Acta Mater., **122**, 92 (2017). DOI: 10.1016/j.actamat.2016.09.042

[7] H. Tanaka, T. Ishikawa, S. Goto, S. Takano, T. Watanabepresenter, M. Yabashi. In: *Proc. IPAC2016,* ed. by C. Petit-Jean-Genaz, Dong Eon Kim, Kyung Sook Kim, In Soo Ko, Kyung Ryul Kim, Volker RW Schaa (Busan, JACoW, 2016), p. 2867–2870. DOI: 10.18429/JACoW-IPAC2016-WEPOW019

[8] A.V. Akimov, Yu.S. Aktershev, V.V. Anashin, A.V. Andiyanov, O.V. Anchugov, M.V. Arcentyeva, P.A. Bak, G.N. Baranov, A.M. Barnyakov, A.M. Batrakov, O.V. Belikov, L.L. Belova, E.A. Bekhtenev,V.I. Bukhtiyarov, A.V. Bogomyakov, V.M. Borin, D.B. Burenkov, D.S. Vinnik, V.N. Volkov, E.S. Vonda, K.M. Gorchakov, K.A. Grishina, D.S. Gurov, G.A. Gusev, B.A. Dovzhenko, E.N. Dementyev, A.I. Erokhin, A.A. Zharikov, K.V. Zhilyaev, A.A. Zhukov, A.N. Zhuravlev, K.V. Zolotarev, N.A.Zolotukhina, Ya.V. Zubavichus, S.E. Karnaev, G.V. Karpov, K.Yu. Karyukina, V.D. Kashkin, V.A. Kiselev, V.V. Kobets, E.S. Kotov, V.Ya Korchagin, A.A. Krasnov, V.S. Krapivin, S.A. Krutikhin, V.S. Kuzminykh, G.N. Kulipanov, I.V. Kuptsov, G.Ya Kurkin, A.E. Levichev, E.B. Levishev, D.V. Leshonok, (Dorokhova), P.V. Logachev, Yu.I. Maltseva, Ma syao Chao, N.A. Mezentsev, O.I. Meshkov, N.V. Mityanina, I.A. Morozov, A.A.Morsin, S.A. Nikitin, D.A. Nikiforov, B.K. Ovchar, I.N. Okunev, A.V. Pavlenko,

O.A. Pavlov, A.Yu Pakhomov, V.M. Petrov, S.L. Pivovarov, P.A. Piminov, A.V. Polyansky, D.N. Pureskin, D.F. Reshetov, V.V. repkov, E.A. Rotov, T.V. Rybitskaya, S.L. Samoilov, I.K. Sedlyarov, A.M. Semenov, D.V. Sen'kov, L.E. Serdakov, Sh.R. Signatulin, S.V. Sinyatkin, M.A. Skamarokha, A.A. Starostenko, A.G. Tribendis, A.V. Utkin, M.G. Fedotov, A.S. tsyganov, A.D. Shiyankov, D.A. Shvedov, V.A. Shkaruba, K.S. Shtro, N.S. Shchegolkov. V sb.: *Tekhnologicheskaya infrastruktura sibirskogo kol'tsevogo istichnika fotonov „SKIF“,* pod. red. K.I. Shifer (Institut kataliza SO RAN, Novosibirsk, 2022), s. 98–179 (in Russian)

[9] N.I. Chkhalo, M.N. Drozdov, E.B. Kluenkov, A.Ya. Lopatin, V.I. Luchin, N.N. Salashchenko, N.N. Tsybin, L.A. Sjmaenok, V.E. Banine, A.M. Yakunin. J. Micro. Nanolithogr. MEMS MOEMS., **11** (2), 021115 (2012). DOI: 10.1117/1.jmm.11.2.021115

[10] C. Zoldesi, K. Bal, B. Blum, G. Bock, D. Brouns, F. Dhalluin, N. Dziomkina, J.D.A. Espinoza, J. de Hoogh, S. Houweling, M. Jansen, M. Kamali, A. Kempa, R. Kox, R. de Kruif, J. Lima, Y. Liu, H. Meijer, H. Meiling, I. van Mil, M. Reijnen, L. Scaccabarozzi, D. Smith, B. Verbrugge, L. de Winters, X. Xiong, J. Zimmerman. Prog. on EUV Pellicle Dev. Extreme Ultraviolet (EUV) Lithography V. SPIE, **9048** (90481N), 430 (2014). DOI: 0.1117/12.2049276

[11] S.Yu. Zuev, A.Ya. Lopatin, V.I. Luchin, N.N. Salashchenko, D.A. Tatarskiy, N.N. Tsybin, N.I. Chkhalo. Tech. Phys., **68** (3), S630 (2023). DOI: 10.1134/S106378422390098X

[12] J.L. Yue, Y.S. Yin, G.Y. Li. Adv. Mater. Res., **79**, 489 (2009). DOI: 10.4028/www.scientific.net/AMR.79-82.489

[13] E.O. Filatova, S.S. Sakhonenkov, A.V. Solomonov, R.M. Smertin, V.N. Polkovnikov. Appl. Surf. Sci., **644**, 158791 (2024). DOI: 10.1016/j.apsusc.2023.158791

[14] P.E. Diehl, M.W. Lund, D.W. Madsen, L.C. McIntyre, D.J. Smith. Thin Solid Films, **239** (1), 57 (1994). DOI: 10.1016/0040-6090(94)90108-2

[15] R. Yoshimoto, Y. Nogi, R. Tamura, S. Takeuchi. Mater. Sci. Eng., **449**, 260 (2007). DOI: 10.1016/j.msea.2006.02.365

[16] V.A. Shkaruba, A.V. Bragin, A.A. Volkov, A.I. Erokhin, A.V. Zorin, F.P. Kazantsev, P.V. Kanonik, N.A. Mezentsev, A.N. Safronov, A.A. Sedov, O.A. Tarasenko, S.V. Khrushchev, V.M. Tsukanov. Phys. Part. Nucl. Lett., **20** (4), 904 (2023). DOI: 10.1134/S1547477123040623

[17] E.I. Glushkov, I.V. Malyshev, E.V. Petrakov, N.I. Chkhalo, Yu.V. Khomyakov, Ya.V. Rakshun, V.A. Chernov, I.P. Dolbnya. J. Surf. Investig., **17** (1), 233 (2023). DOI: 10.1134/S1027451023070133

[18] Electronic source. Available at: https://htw-germany.com/en/material. Date of access 15.05.2024

[19] T. Tanaka. J. Synchrotron Rad., **28** (4), 1267 (2021). DOI: 10.1107/S1600577521004100

[20] M. Balat-Pichelin, J.F. Robert, J.L. Sans. Appl. Surf. Sci., **253** (2), 778 (2006). DOI: 10.1016/j.apsusc.2006.01.007

[21] E. Madenci, I. Guven. *The Finite Element Method and Applications in Engineering Using ANSYS®* (Springer, 2015), DOI: 10.1007/978-1-4899-7550-8

Translated by E.Ilinskaya